Progress In Electromagnetics Research B, Vol. 9, 215–230, 2008

ADAPTIVE GENETIC ALGORITHM BASED SOURCE IDENTIFICATION WITH NEAR-FIELD SCANNING METHOD

B. Liu, L. Beghou, and L. Pichon

Laboratoire de Génie Electrique de Paris
CNRS UMR8507; SUPELEC; UPMC Univ Paris 06; Univ Paris-Sud
P. O. Box 91192 Gif-sur-Yvette, France

F. Costa

Laboratoire SATIE
CNRS UMR 8029; UnivSud; IUFM Créteil
Ecole Normale Supérieure de Cachan, 94230 Cachan, France

Abstract—With the global search method of adaptive genetic algorithm (GA), an improved methodology is proposed to identify the equivalent radiating dipoles of real sources on substrates such as printed circuit boards (PCB) and then to regenerate the radiating far field. This methodology is based on a set of elemental electric- and magnetic dipoles which model the real sources. The numbers, positions and orientations as well as the elevations of each dipole are positioned by adaptive GA based on the comparison between the simulated and measured magnetic field. The methodology provides a possible way to identify the radiating source of planar circuits with ground plane.

1. INTRODUCTION

With the rapid development of modern electronic device design, the effects of electromagnetic radiation on board become non-negligible and may deteriorate the performances of devices. For this reason, the research on modeling of source identification has become a critical point. This is particularly important for Switched Mode Power Supplies (SMPS). The devices are DC-DC converters and allow obtaining good efficiency with high power-weight and power-volume ration. One way to build adequate models is to design a prototype at the beginning and adjust the positions of the components according to

the measured interference and redo the operations until the interference meets the requirements. This leads to cost inflations and interferences with the production schedule. Another way is to build an equivalent model on set of elemental dipoles substituting the real sources to generate the same radiation field as the measurement.

Several successful works on this topic have been published: Kralicek et al. studied the emitting sources using multipole expansion [1]. Petre and Sarkar et al. applied the equivalent currents approach in antenna design to calculate the far-field from the near-field radiation by using conjugate gradient method [2–4]. Sijher and Kishk used binary GA optimization method to simulate antennas from near-field distribution by a set of infinitesimal dipoles [5]. A 2D model with dipoles located in a plane was put forward by Gilabert et al. using the near-field scanning method [6]. Regué et al. used genetic algorithm to find out the source distribution and predict the far-field radiations [7]. De Daran et al. modeled the coupling phenomena on electronic board and evaluated the radiated emission [8].

In this paper, a methodology based on the substitution of radiating dipoles for real sources is presented. The parameters of each equivalent dipole, i.e., the type, number, position, elevation, orientation and the moments, are founded by an adaptive GA supposing that the equivalent dipoles operate at the same frequency as the real sources. This methodology focuses on identifying the source distribution in a three-dimension (3D) space and advantages in: 1) it is independent of the traditional image theory and applicable to low frequency issues comparing to [7], 2) each parameter of these dipoles is not predefined and variable within a bound, 3) three kinds of approaches are included: using only electric dipoles, using only magnetic dipoles and using both types of dipoles, 4) a self-defined adaptive GA other than standard GA is adopted, the procedures of selection, crossover and mutation are adjusted adaptively and optimized for multi-parameter search.

The methodology will be illustrated in next section followed by the introduction of adaptive GA in section three and is validated by simulation and experiment in section four. Finally, a conclusion is given.

2. DESCRIPTION OF THE METHODOLOGY

In printed circuit boards, electromagnetic interference (EMI) is usually generated by straight- and loop currents, which can be modeled as electric- and magnetic dipoles. We aim to find those equivalent dipoles relevant to an electric device under test (DUT) that can generate the same field as the real source of the DUT. This is achieved by minimizing

the difference between the simulated field and the measured field using adaptive GA.

The expressions of the radiating field generated by elemental dipoles are well known and can be represented as (1)–(2) and the total field generated by N dipoles is the superposition of the elementary fields generated by the dipoles:
for an electric dipole

$$\mathbf{H}(\mathbf{r}_{mes}) = -\frac{jk_e}{4\pi}\left(1+\frac{j}{k_eR}\right)\frac{\mathbf{M}\times\mathbf{R}e^{jk_eR}}{R^2} \tag{1}$$

for a magnetic dipole

$$\begin{aligned}\mathbf{H}(\mathbf{r}_{mes}) = \frac{k_e^2}{4\pi}\Bigg[&\left(1+\frac{j}{k_eR}-\frac{1}{(k_eR)^2}\right)\mathbf{M}\\ &-\left(1+\frac{3j}{k_eR}-\frac{3}{(k_eR)^2}\right)\frac{(\mathbf{R}\cdot\mathbf{M})\,\mathbf{R}}{R^2}\Bigg]\frac{e^{jk_eR}}{R};\end{aligned} \tag{2}$$

where, $\mathbf{R} = \mathbf{r}_{mes} - \mathbf{r}_s$, $R = ||\mathbf{r}_{mes} - \mathbf{r}_s||$, $\mathbf{r}_{mes}$ is the position of the measurement point, $\mathbf{r}_s$ is the position of the source point (Fig. 1), i.e., the dipole, and $\mathbf{M}$ is the moment of the dipole.

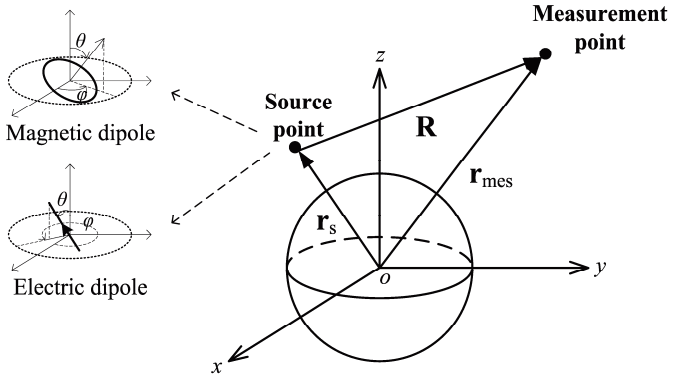

Figure 1. The definitions of equivalent radiating dipoles.

Generally, the metallic layers of PCB are non-perfect electric conductor at low frequency, which means the image theory is not valid due to skin effect. In our methodology, the position, elevation and orientation of image dipole are supposed to still correspond to its original dipole following the image theory except the amplitude of moment is different from that of the real dipole. There are seven

parameters for each dipole (3):

$$para\_vect = [x_i, y_i, z_i, \theta_i, \phi_i, \mathbf{M}, \mathbf{M}_{im}] \tag{3}$$

where, $[x_i,\ y_i,\ z_i]$ is the geometrical center position of dipole i, $[\theta_i,\ \varphi_i]$ is its elevation and orientation and $[M,\ M_{im}]$ is the corresponding real- and image magnetic (or electric) moment. Therefore, a set of N radiating dipoles can be represented as N 1×7 parameter vectors and the total radiated magnetic field generated by these dipoles at one measurement point can be expressed as (4):

$$\mathbf{H}_{total} = \sum_{i=1}^{N} \mathbf{H}_i(r_{mes}, x_i, y_i, z_i, \theta_i, \phi_i, \mathbf{M}_i, \mathbf{M}_{imi}) \tag{4}$$

where, $\mathbf{H}_{total}$ is the magnetic field at the measurement point generated by all elementary dipoles and $\mathbf{H}_i$ is the field of dipole i.

An adaptive genetic algorithm was used in the methodology to search for the optimal set of dipoles, the radiating field of which (H_s) is closest to that measured field (H_m), and the difference $||H_s - H_m||$ will reach the minimum. The algorithm will evaluate the inverse of the difference to achieve a maximal fitness value as shown in (5) and the fitness is calculated according to the measured data of every point of the measuring grid:

$$fitness = \left[\sum_{j=1}^{3} \|H_{sj} - H_{mj}\| \right]^{-1} \tag{5}$$

where, H_j, $j = 1, 2, 3$ corresponds to H_x, H_y and H_z, separately.

3. GENETIC ALGORITHM

3.1. Standard Genetic Algorithm

Genetic algorithms are probabilistic search techniques based on the principles of biological evolution [9, 10]. In general, a standard GA has five basic steps [9] (see Fig. 2): 1) to create a genetic representation of potential solutions to the problem, 2) to create a population working as an initial set of potential solutions, 3) to build an evaluation function rating solutions in terms of their fitness values, 4) to define the genetic operators that alter the genetic composition of offspring (selection, crossover, mutation, etc.), 5) to adjust the parameters of GA (population size, probabilities of genetic operators, etc.).

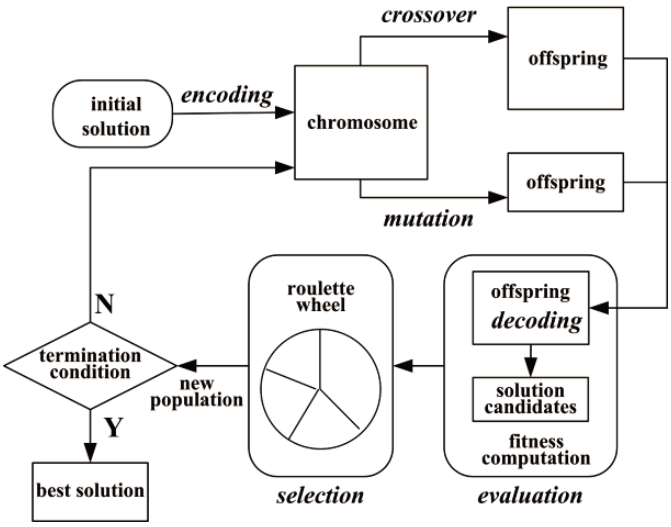

Figure 2. The general structure of standard genetic algorithm.

3.2. Adaptive Genetic Algorithm for Multi-parameter

Standard GA shows good performance in solving global optimization problems. However, the invariabilities of its parameters will conflict with the instinct of GA, i.e., dynamic adaptation. Usually, standard GA converges fast to the sub-domain that contains the global optimum, after that, it will probably become very time-consuming to locate the global optimum in local searching process [11, 12]. Different kinds of genetic algorithms have been used to solve electromagnetic problems [13–21], and in this work, an adaptive GAis developed from standard GAand optimized for solving multi-parameter optimization problems.

3.2.1. Realization of Adaptive Selection

In the selection procedure of GA, the superior individuals in current generation will be copied to next generation according to the principles of natural selection, while those inferior will be filtered out. The ratio of the best individual's selection probability to the average selection probability of all individuals in the selection pool is called selection pressure. In GA, at the beginning stages, there are big differences between individuals and small selection pressure can keep the good effects of less-fitness individuals, but as the generation number increases, high selection pressure is preferred to accelerate the

convergence in that only small differences remain among the evolved individuals. So the constant selection strategy used in standard GA is not capable of dynamic selections. Here an adaptive power selection strategy (6) is utilized in our methodology to alter the selection pressure by a power function, i.e., $\alpha(t)$, adaptively.

$$P\{Y_i = X_j(t)\} = \frac{n\left(X_j(t)\right) J^{\alpha(t)}\left(X_j(t)\right)}{\sum_{k=1}^{N} J^{\alpha(t)}\left(X_k(t)\right)} \tag{6}$$

where, $\{Y_1, Y_2, \ldots, Y_n\}$ is the new population consists in the newly selected individuals, $P\{Y_i = X_j(t)\}$ means the probability of being selected for $X_j(t)$, $n(X_j(t))$ is the number of $X_j(t)$ in current population, $J(X_j(t))$ is the fitness of the $X_j(t)$, $\alpha(t)$ is a monotonously increasing sequence of positive real and $\sum J(X_k(t))$ is the sum of all the individuals in current population.

3.2.2. Realization of Adaptive Crossover

In GA, the global searching is in charge of crossover, which creates new chromosomes (offsprings) by combining parts from two chromosomes with a probability (P_c). Standard GA uses a constant P_c, which takes effect only in parts of the evolution time. For the same reason as adaptive selection, P_c should be small at the beginning to limit the influence of crossover and be big after that to strengthen crossover to avoid evolution stagnancy.

In our methodology, P_c will adjust itself automatically according to the status of evolution: if the mean fitness in the passing several generations keep increasing visibly, P_c will decrease, otherwise, it will increase (7).

$$P_{cnew} = \frac{\left(\sum_{j=i-1-N}^{i-1} \Delta f_i\right) \cdot P_c}{\sum_{j=i-N}^{i} \Delta f_i} \tag{7}$$

where, P_{cnew} is the adaptively adjusted probability of crossover, P_c is the original probability of crossover, i is the number of current generation, and Δf_i is the difference between the mean fitness of individuals in the immediate N generations.

3.2.3. Realization of Adaptive Mutation

In GA, mutation creates offspring by inversing the value of randomly fixed position of a chromosome selected with a constant probability (P_m). The use of constant P_m in standard GA limits the effect of mutation on the evolution of population due to the constant and small mutation area. To avoid such a drawback, the algorithm was improved in our work by assign each chromosome a P_m to make sure that the good-fitness chromosomes will have small $P_m s$ while bad-fitness chromosomes will have big $P_m s$ (8). In this way, the bad-fitness chromosomes will be mutated more and be accelerated towards the optimal solution and good-fitness chromosomes only need to undergo gentle mutations so as not to change their evolution directions.

$$P_{mnew} = P_m \cdot \frac{\overline{f}}{f_j}, \qquad j = 1, 2, \ldots, N \tag{8}$$

where, f_j is the fitness of chromosome j, $\bar{f}$ is the mean fitness of the current population, P_{mnew} is the adaptively adjusted probability of mutation and P_m is the original probability of mutation.

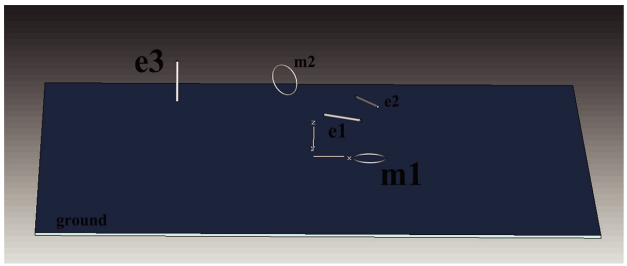

Figure 3. The model of two magnetic dipoles and three electric dipoles.

3.2.4. Improvement for Multi-parameter Optimization

Although GA has a good efficiency in optimizing single-parameter problems, its efficiency will decrease when deals with multi-parameter problems. One possible reason is that the parameters or its corresponding codes don't have the same probability to evolve. In our methodology, the uniform crossover operation is introduced to crossover all the gene with the same probability so that equal-probability searches can be available in all solution space of the parameters. The details of uniform crossover operation can be referred in [12].

3.2.5. Keep the Best N Individuals

In the adaptive GA we used, the individuals in current generation with the N best fitness are kept and transferred to the next generation. This operation can avoid those better solutions (individuals) being wiped off when undergoing selection, crossover and mutation, so that increase the speed of convergence.

With above improvements on the genetic algorithm, the methodology can efficiently solve the multi-parameter issues, as validated in following Section 4.

4. NUMERICAL & EXPERIMENTAL VALIDATION

4.1. Validation by Simulation

To test the ability of the methodology to work at low frequency with non-perfect ground plane, a model working at 50 kHz was built, which consists of two magnetic dipoles and three electric dipoles above a 20 cm × 20 cm ground plane (see Fig. 4).

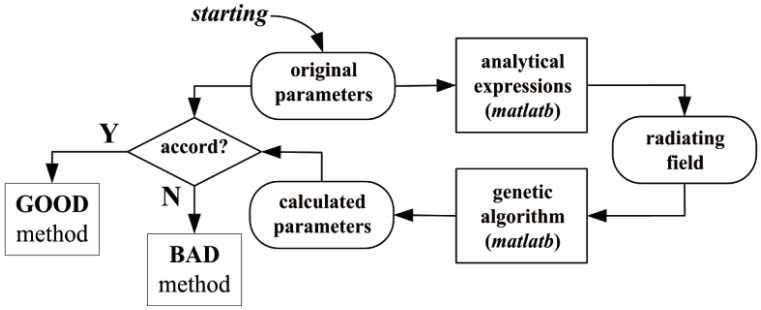

Figure 4. The flow of validation by analytical results.

The model generates a radiating magnetic field (marked as 'ORIGINAL') and it will be analyzed by an adaptive GA and a standard GA for comparison, supposing that all the values of the parameters (3) are unknown except the constraints of lower and upper bounds listed in Table 1 and the initial values of GA operators are listed in Table 2.

The comparison between the original magnetic field and that generated by the dipoles found by both GAs is shown in Fig. 5, where we can find the big differences between the 'SGA' case and the 'ORIGINAL' case and the field of 'AGA' is much better than that of 'SGA'. The parameters of the original dipoles and those found by

Table 1. Bounds on parameters.

Item	x_0 (m)	y_0 (m)	z_0 (m)	θ (rad)	φ (rad)	M	M_{im}
Lower bound	-5.0×10^{-2}	-5.0×10^{-2}	0	0	0	0	0
Upper bound	5.0×10^{-2}	5.0×10^{-2}	3.0×10^{-2}	PI	2*PI	5.0×10^{-3}	5.0×10^{-3}
Precision	1×10^{-3}	1×10^{-3}	1×10^{-3}	1×10^{-2}	1×10^{-2}	1×10^{-5}	1×10^{-5}

Table 2. Initialization of genetic algorithm parameters.

GA Type	P_c	P_m	Population Size	Iteration Num
Standard GA	0.70	0.0142	200	1000
Adaptive GA	0.70	0.0142	200	100

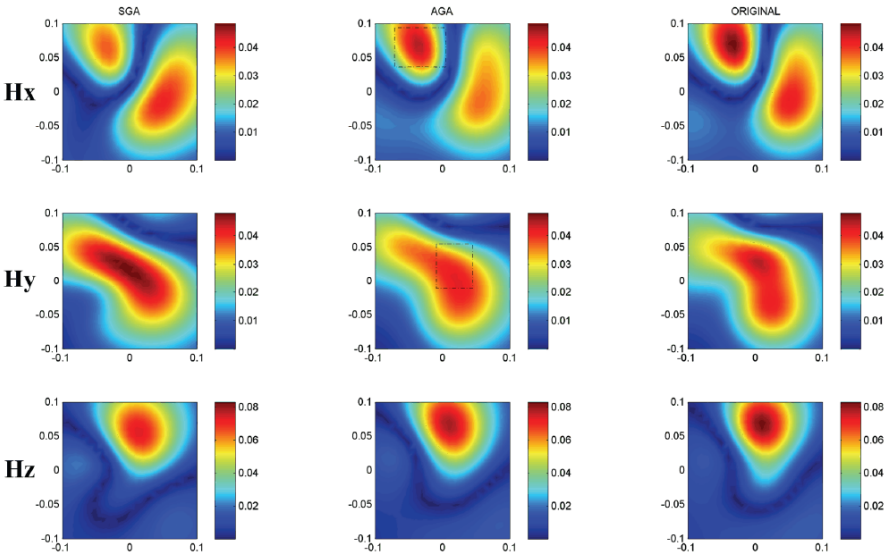

Figure 5. Field distribution of the original sources and the equivalent dipoles found AGA and SGA.

adaptive GA are listed in Table 3, the similarities shown in which illustrate that the adaptive GA worked effectively.

The convergences of adaptive GA and standard GA used in above case are illustrated in Fig. 6. Due to the invariable crossover- and mutation probabilities, single-parameter mechanism as well as the

constant selection pressure, the fitness calculated by standard GA undulates sharply as the iteration goes, which is caused by the lack of "keeping the best N individuals" operation when both the SGA and AGA case have the genetic operators of the same initial values. So the SGA case only achieved a fitness of 0.2041. With the improvements mentioned in 3.2, the adaptive GA got a smooth evolution curve and achieved a much better fitness value at 0.4410 effectively, which accords to the bigger similarity between 'AGA' and 'ORIGINAL' cases in Fig. 5.

Table 3. Data of validation by numerical simulation.

Dipole	x_0 (m)	y_0 (m)	z_0 (m)	θ (rad)	φ (rad)	M	M_{im}
$\boldsymbol{e1}$ (Original)	1.0×10^{-2}	-2.0×10^{-2}	2.0×10^{-2}	1.5708	1.0472	5.0×10^{-3}	3.0×10^{-3}
$\boldsymbol{e1}$ (AGA)	0.04×10^{-2}	-5.00×10^{-2}	2.50×10^{-2}	1.9673	0	1.7624×10^{-3}	0.3368×10^{-3}
$\boldsymbol{e2}$ (Original)	2.0×10^{-2}	2.0×10^{-2}	1.5×10^{-2}	1.5708	0.5236	4.0×10^{-3}	3.0×10^{-3}
$\boldsymbol{e2}$ (AGA)	4.29×10^{-2}	-2.56×10^{-2}	1.21×10^{-2}	1.5738	1.1731	4.6965×10^{-3}	1.4681×10^{-3}
$\boldsymbol{e3}$ (Original)	-5.0×10^{-2}	1.0×10^{-2}	2.5×10^{-2}	0	4.7124	2.0×10^{-3}	1.0×10^{-3}
$\boldsymbol{e3}$ (AGA)	-2.95×10^{-2}	1.22×10^{-2}	2.02×10^{-2}	0.3873	2.9297	1.9372×10^{-3}	1.5912×10^{-3}
$\boldsymbol{m1}$ (Original)	2.0×10^{-2}	-2.0×10^{-2}	5.0×10^{-3}	0	0.5236	5.0×10^{-4}	3.0×10^{-4}
$\boldsymbol{m1}$ (AGA)	1.18×10^{-2}	5.00×10^{-2}	0	0.0430	3.1385	8.6566×10^{-4}	5.4726×10^{-4}
$\boldsymbol{m2}$ (Original)	-1.0×10^{-2}	5.0×10^{-2}	1.5×10^{-2}	1.0472	0.7854	4.0×10^{-4}	3.0×10^{-4}
$\boldsymbol{m2}$ (AGA)	-2.32×10^{-2}	5.00×10^{-2}	0.32×10^{-2}	1.8075	0.7862	4.7016×10^{-4}	1.2417×10^{-4}

There are still also several little differences between 'AGA' case and 'ORIGINAL' case, the corresponding areas of which are enclosed by dashed frames (see Fig. 5). There are two possible causes: 1) the complete uncertainty of elevations and orientations leads to more diversities than those in planar circuit, where the current trace are usually in vertical or horizontal direction, so there are much more possible sets of dipoles that can radiate similar field, 2) though adaptive GA overruns standard GA here, the iteration is insufficient to guarantee the convergence., which means the adaptive algorithm can converge to a better result with more iterations.

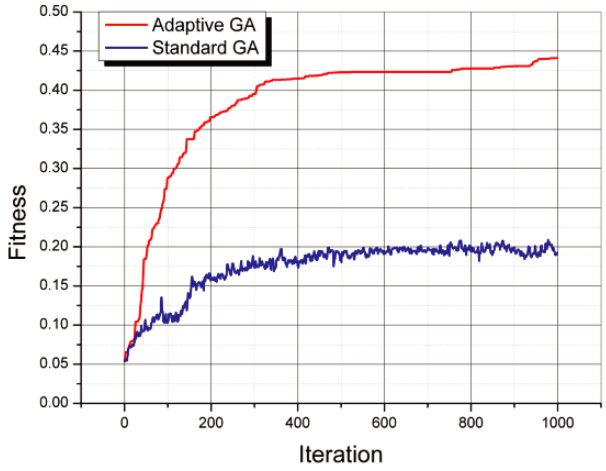

Figure 6. The convergences of adaptive GA and standard GA.

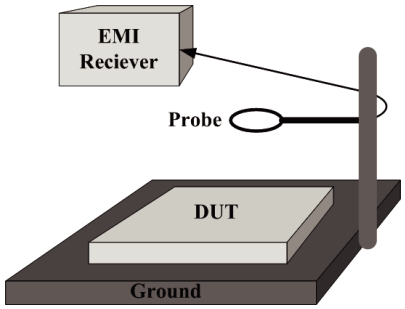

Figure 7. The configuration of the test bench.

4.2. Application of the Methodology to a DC-DC Converter

4.2.1. Description of the Test Bench

The test bench used in the measurement is a near-field scan system mounted on a 2D displacement table as illustrated in Fig. 7. It consists of a ground plane (60 cm × 50 cm) and an EMI receiver (9 kHz–2.9 GHz) equipped with a magnetic field probe of a 0.5 cm radius [22–26]. The DUT is fixed on the ground plane and the probe is placed 20 cm above it. The measurement of the DUT via the probe is under the control of a computer and the measured area has a dimension of 9.5 cm × 17.5 cm in XOY plane with steps of 5 mm in both directions. The final measured magnetic field is recorded by the EMI receiver.

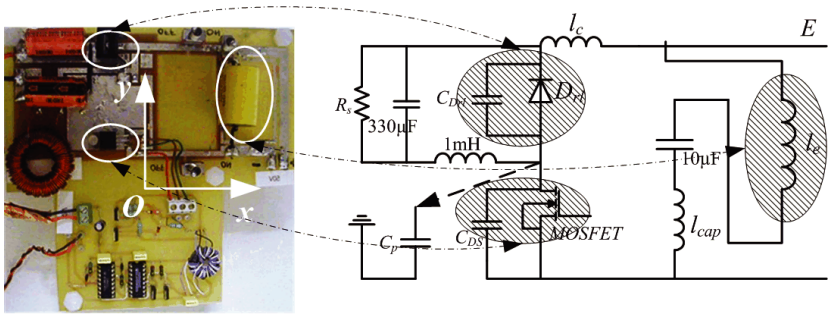

Figure 8. The DC-DC converter under test.

4.2.2. Description of the Device under Test

DC-DC converters are widely used in power supply systems, with which good efficiency, high power-weight and power-volume ratio can be obtained at the cost of conducted and radiated losses caused by switching operations. Fig. 8 shows a DC-DC structure, i.e., the device under test (DUT) here, which is a buck chopper fed by 50 V voltage source at a switching frequency of 50 kHz. The load current is 2 A and the duty cycle of the diode in the circuit is 0.5.

4.2.3. Experimental Results

As shown in Fig. 9, the measured data correspond to the three pictures of the right column marked as 'Measurement'. The methodology switched three approaches, i.e., only using electric dipoles, only using magnetic dipoles and using both kinds of dipoles, and found from the analysis of given measured magnetic field that only radiating magnetic dipoles was needed. The simulated field generated by the magnetic dipole found by the methodology here is illustrated in the left column in Fig. 9 and the details are the listed in Table 4.

Table 4. Data of validation by near-field scanning data (50 kHz).

GA type	x_0 (m)	y_0 (m)	z_0 (m)	θ (rad)	φ (rad)	M	M_{im}
simulation results	**0.010**	**0.038**	**0.135**	**0.058**	**0.554**	$\mathbf{3.9370 \times 10^{-5}}$	$\mathbf{3.9370 \times 10^{-5}}$
simulation precision	1×10^{-3}	1×10^{-3}	1×10^{-3}	1×10^{-3}	1×10^{-3}	1×10^{-5}	1×10^{-5}

According to the field distribution in Fig. 9 and the data in Table 4, there is only one magnetic dipole dominating the radiation

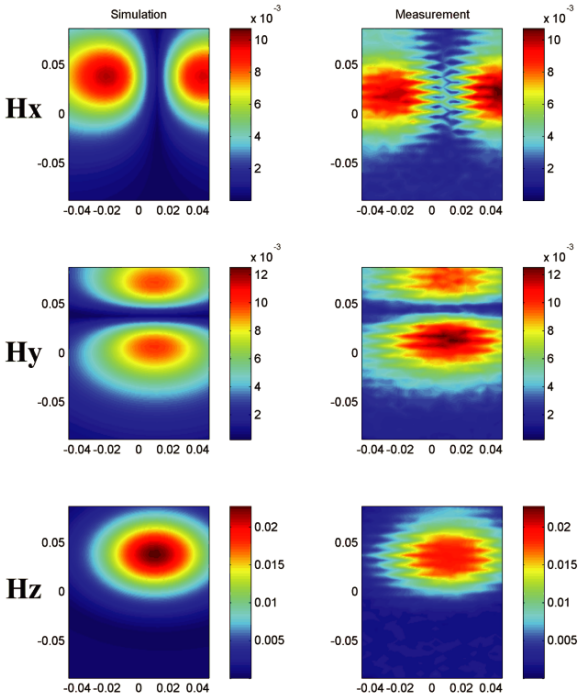

Figure 9. The measured data and the simulated results.

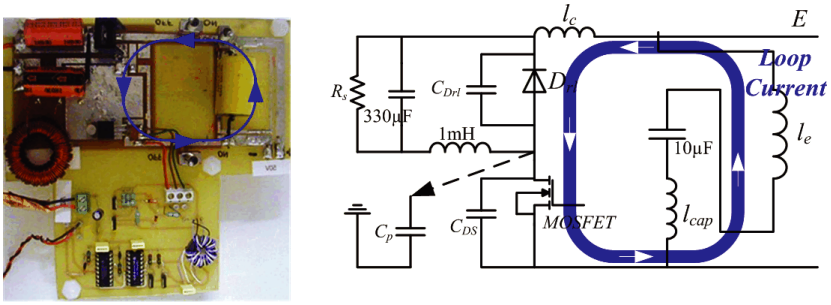

Figure 10. The radiating loop current in the DUT.

with a position of (1.0 cm, 3.8 cm) in XOY plane. As for its position in Z direction, i.e., $z0$, the value is 13.5 cm and less than the distance between the probe and the ground plane, which probably caused by the big size of low-frequency components mounted on the PCB so that several segments of the current trace shown in Fig. 10 are not in the

XOY plane, but in a 3D space, which can also be judged from the non-zero elevation, i.e., $\theta = 0.058$ rad (3.3 degree).

5. CONCLUSION

An improved methodology based on adaptive GA is proposed for source identification from near-field scanning magnetic field. The method is based on the substitution of real radiating sources by equivalent dipoles distributed in a 3D area. The adoption of adaptive GA accelerated the convergence and avoided premature convergence. The applicability of the methodology is validated by a simulation model and near-field scanning measurement.

ACKNOWLEDGMENT

The authors acknowledge Cécile Labarre and Ouafae Aouine from Ecole des Mines de Douai for providing the experimental results relevant to the power converter used in this work.

REFERENCES

1. Kralicek, P., W. John, and H. Garbe, "Modeling electromagnetic emission of integrated circuits for system analysis," *DATA Conf.*, Munich, Germany, Mar. 2001.
2. Petre, P. and T. K. Sarkar, "Planar near-field to far-field transformation using an equivalent magnetic current approach," *IEEE Trans. Antennas Propag.*, Vol. 40, No. 11, 1348–1355, Nov. 1992.
3. Taaghol, A. and T. K. Sarkar, "Near-field to near/far-field transformation for arbitrary near-field geometry utilizing an equivalent magnetic current," *IEEE Trans. Electromag. Compat.*, Vol. 38, No. 3, 536–542, Aug. 1996.
4. Sarkar, T. K. and A. Taaghol, "Near-field to near/far-field transformation for arbitrary near-field geometry utilizing an equivalent electric current and MOM," *IEEE Trans. Electromagn. Compat.*, Vol. 47, No. 3, 566–573, Mar. 1999.
5. Sijher, T. S. and A. A. Kishk, "Antenna modeling by infinitesimal dipoles using genetic algorithms," *Progress In Electromagnetics Research*, PIER 52, 225–254, 2005.
6. Vives-Gilabert, Y., C. Arcambal, A. Louis, F. de Daran, P. Eudeline, and B. Mazari, "Modeling magnetic radiations of

electronic circuits using near-field scanning method," *IEEE Trans. Electromagn. Compat.*, Vol. 49, No. 2, 391–400, 2007.

7. Regué, J.-R., M. Ribó, J. M. Garrell, and A. Martin, "A genetic algorithm based method for source identification and far-field radiated emissions prediction from near-field measurements for PCB characterization," *IEEE Trans. Electromagn. Compat.*, Vol. 43, No. 4, 520–530, Nov. 2001.
8. de Daran, F., J. Chollet-Ricard, F. Lafon, and O. Maurice, "Prediction of the field radiated at one meter from PCB's and microprocessors from near EM field cartography," *Proc. IEEE Int. Symp. Electromagn. Compat.*, Vol. 1, 479–482, Istanbul, Turkey, May 2003.
9. Gen, M. and R. Cheng, *Genetic Algorithms and Engineering Optimization*, Ch. 1, John Wiley & Sons, New York, 2000.
10. Michalewicz, Z., *Genetic Algorithms + Data Structures = Evolution Programs*, 3rd edition, Part 1, Springer-Verlag, New York, 1996.
11. Kitano, H., "Empirical studies on the speed of convergence of the neural network training by genetic algorithm," *Proc. of AAAI-90*, 1990.
12. Qi, X. and F. Palmieri, "Theoretical analysis of evolutionary algorithms with an infinite population size in continuous space part II: Analysis of the diversification role of crossover," *IEEE Trans. Neural Netw.*, Vol. 5, No. 1, Jan. 1994.
13. Donelli, M., S. Caorsi, F. D. Natale, et al., "A versatile enhanced genetic algorithm for planar array design," *J. of Electromagn. Waves and Appl.*, Vol. 18, No. 11, 1533–1548, 2004.
14. Lucci, L., R. Nesti, G. Pelosi, et al., "Phase centre optimization in profiled corrugated circular horns with parallel genetic algorithms," *Progress In Electromagnetics Research*, PIER 46, 127–142, 2004.
15. Nyobe, E. N. and E. Pemha, "Propagation of a laser beam through a plane and free turbulent heated air flow: Determination of the stochastic characteristics of the laser bean random direction and some experimental results," *Progress In Electromagnetics Research*, PIER 53, 31–53, 2005.
16. Chen, X., K. Huang and X. B. Xu, "Microwave imaging of buried inhomogeneous objects using parallel genetic algorithm combined with FDTD method," *Progress In Electromagnetics Research*, PIER 53, 283–298, 2005.

17. Lu, Y. Q. and J. Y. Li, "Optimization of broadband top-load antenna using micro-genetic algorithm," *J. of Electromagn. Waves and Appl.*, Vol. 20, No. 6, 793–801, 2006.
18. Tian, Y. B. and J. Qian, "Ultra-conveniently finding multiple solutions of complex transcendental equations based on genetic algorithm," *J. of Elecgtromagn. Waves and Appl.*, Vol. 20, No. 4, 475–488, 2006.
19. Lu, Y. Q. and J. Y. Li, "Optimization of broadband top-load antenna using micro-genetic algorithm," *J. of Elecgtromagn. Waves and Appl.*, Vol. 20, No. 6, 793–801, 2006.
20. Su, D. Y., D. M. Fu, and D. Yu, "Genetic algorithms and method of moments for the design of PIFAs," *Progress In Electromagnetics Research Letters*, Vol. 1, 9–18, 2008.
21. Nyobe, E. N. and E. Pemha, "Shape optimization using genetic algorithms and laser beam propagation for the determination of the diffusion coefficient in a hot turbulent jet of air," *Progress In Electromagnetics Research B*, Vol. 4, 211–221, 2008.
22. Béreau, E., "Measurement bench for electromagnetic near field characterization of power electronics devices," *IEEE Symp. on Embedded EMC*, 2emc, Rouen, 2005.
23. Baudry, D., A. Louis, and B. Mazari, "Characterization of the open-ended coaxial probe used for near-field measurements in EMC applications," *Progress In Electromagnetics Research*, PIER 60, 311–333, 2006.
24. Aouine, O., C. Labarre, F. Costa, P. Baudesson, and J. Ecrabey, "Identification of the radiated sources inside a variable speed drive from near-field measurements," *EMC 2007, EMC Methodology Session 6,5E*, Oct. 19, 2007.
25. Aouine, O., C. Labarre, and F. Costa, "Measurement and modeling of the magnetic near field radiated by a buck chopper," *IEEE Trans. EMC*, Vol. 50, No. 2, 445–449, May 2008.